Thin Solid Films 579 (2015) 81–88

Contents lists available at ScienceDirect

Thin Solid Films

journal homepage: www.elsevier.com/locate/tsf

Fabrication of solid-state thin-film batteries using $LiMnPO_4$ thin films deposited by pulsed laser deposition

Daichi Fujimoto [a,b], Naoaki Kuwata [a,*], Yasutaka Matsuda [a], Junichi Kawamura [a], Feiyu Kang [b]

[a] Institute of Multidisciplinary Research for Advanced Materials, Tohoku University, Katahira 2-1-1, Aoba-ku, Sendai 980-8577, Japan
[b] Key Laboratory of Advanced Materials (MOE), School of Materials Science and Engineering, Tsinghua University, Beijing 100084, China

ARTICLE INFO

Article history:
Received 9 March 2014
Received in revised form 15 January 2015
Accepted 13 February 2015
Available online 20 February 2015

Keywords:
Lithium manganese phosphate
All solid-state battery
Pulsed laser deposition
Chemical diffusion coefficient
Electronic conductivity
Olivine-type structure
Amorphous solid electrolyte

ABSTRACT

Solid-state thin-film batteries using $LiMnPO_4$ thin films as positive electrodes were fabricated and the electrochemical properties were characterized. The $LiMnPO_4$ thin films were deposited on Pt coated glass substrates by pulsed laser deposition. In-plane X-ray diffraction revealed that the $LiMnPO_4$ thin films were well crystallized and may have a texture with a (020) orientation. The deposition conditions were optimized; the substrate temperature was 600 °C and the argon pressure was 100 Pa. The electrochemical measurements indicate that the $LiMnPO_4$ films show charge and discharge peaks at 4.3 V and 4.1 V, respectively. The electrical conductivity of the $LiMnPO_4$ film was measured by impedance spectroscopy to be 2×10^{-11} S cm^{-1} at room temperature. The solid-state thin-film batteries that show excellent cycle stability were fabricated using the $LiMnPO_4$ thin film. Moreover, the chemical diffusion of the $LiMnPO_4$ thin film was studied by cyclic voltammetry. The chemical diffusion coefficient of the $LiMnPO_4$ thin film is estimated to be 3.0×10^{-17} cm^2 s^{-1}, which is approximately four orders magnitude smaller than the $LiFePO_4$ thin films, and the capacity of the thin-film battery was gradually increased for 500 cycles.

1. Introduction

The olivine-type $LiMPO_4$ (M = Fe, Mn, Co) proposed by Padhi et al. [1] has been demonstrated to be a promising cathode material for rechargeable Li batteries. Among the olivine-type materials, $LiMnPO_4$ has attracted attention because it has a higher working potential (4.1 V vs. Li/Li$^+$) than $LiFePO_4$ [2,3]. Unfortunately, the rate performance of the olivine-type $LiMnPO_4$ is limited by its poor electronic conductivity [4,5]. Although carbon coating [6,7] and particle size reduction [8–10] have been demonstrated as effective strategies, further understanding of the intrinsic transport properties of $LiMnPO_4$ is required to reveal the factors that predominate the electrochemical properties. Thin-film electrodes are of great interest because they can serve as a simplified model to understand the electrochemical process of active materials [11]. Well-defined thin films are suitable for fundamental research since no binder and conductive additives are included. Moreover, thin-film cathode materials are also essential for all solid-state thin-film batteries (TFBs) [12–15]. Thin-film rechargeable Li batteries have numerous possible applications such as implantable medical devices, remote sensors, and smart cards [16–18].

Numerous studies on the growth of olivine $LiFePO_4$ thin films by radio-frequency (RF) magnetron sputtering [19,20,21], ion beam sputtering [22], pulsed laser deposition (PLD) [23–30], and electrostatic spray deposition (ESD) [31] have been reported. The $LiCoPO_4$ thin films have also been grown by RF magnetron sputtering [32–34], ESD [35], and a sol–gel method [36]. However, very few studies on $LiMnPO_4$ thin films have been reported, possibly due to the difficulty of structure and composition control. Ma and Qin [31] have authored the report on $LiMnPO_4$ thin-films, in which they have reported the application of ESD combined with a sol–gel method. The films were deposited on a stainless steel substrate and then post-annealed at 600 °C to obtain crystalline $LiMnPO_4$. The charge and discharge characteristics were confirmed using liquid electrolytes. The reversible capacity was less than 8 mAh g^{-1}, which is 5% of the theoretical capacity; however, fabrication of solid-state TFBs using $LiMnPO_4$ films has not been reported. ESD films usually have rough surface morphologies, which may cause short-circuit problems in the battery. Thus, physical vapor deposition techniques are preferred to obtain a dense film with uniform thickness.

In this paper, we report the deposition of carbon-free $LiMnPO_4$ thin films on Pt coated SiO_2 glass substrates using a pulsed laser deposition (PLD) technique. One of the most important characteristics in PLD is the ability to realize stoichiometric transfer of ablated material from multi-component targets. This arises from the non-equilibrium nature of the laser ablation process due to absorption of high laser energy density by a small volume of a target material. Since the $LiMnPO_4$ is a multicomponent oxide, PLD is suitable technique for thin-film deposition. Another advantage of PLD is the ability to operate with various background

* Corresponding author.
E-mail address: kuwata@tagen.tohoku.ac.jp (N. Kuwata).

http://dx.doi.org/10.1016/j.tsf.2015.02.041

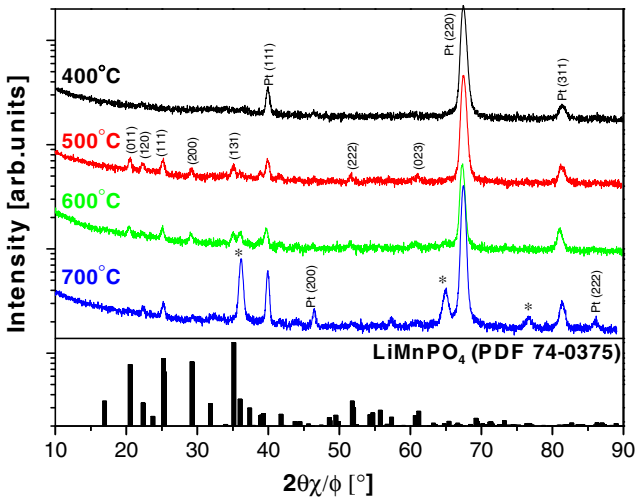

Fig. 1. In-plane X-ray diffraction patterns for $LiMnPO_4$ thin films deposited at substrate temperatures of 400, 500, 600, and 700 °C at 100 Pa Ar pressure. Asterisk (*) shows peaks probably due to manganese oxide.

pressures of gases. Actually, the $LiMnPO_4$ thin films were sensitive to the process gases and the pressure, which were optimized to obtain the best electrochemical properties. The crystal structure, lattice vibration, surface morphology, and electrochemical performance of the $LiMnPO_4$ thin films were characterized. The solid–solid interface between the electrodes and the solid electrolyte is essential for the solid-state battery. A good contact between cathode and solid electrolyte is achieved by sequential PLD process using exchanging different target materials [37]. All solid-state TFBs were fabricated using the $LiMnPO_4$ film as the positive electrode. The TFBs were tested between 3.5 and 4.5 V vs. Li/Li^+, and demonstrated excellent cycle performance for 500 cycles.

2. Experimental details

The $LiMnPO_4$ powder was prepared by hydrothermal reaction at 150 °C for 12 h. The starting chemicals were lithium hydroxide monohydrate ($LiOH \cdot H_2O$), manganese acetate tetrahydrate ($Mn(CH_3COO)_2 \cdot 4H_2O$), and ammonium dihydrogen phosphate ($NH_4H_2PO_4$). The chemicals were placed into an autoclave with distilled water. The molar ratio of Mn and H_2O was 1:15, and the molar ratio of Li, Mn, and P in the precursor solution was set to 1.75:1.0:1.1. The $LiMnPO_4$ powder was ground by wet ball-milling with ethanol and then pressed into 1.66-mm-thick pellets with a diameter of 20 mm using a hydrostatic press. The pellet was then sintered at 800 °C for 10 h in Ar atmosphere. The relative density of the target was 97% of the theoretical density (3.44 g cm^{-3}) of $LiMnPO_4$. The composition ratio of the target was Li:Mn:P = 1.02:1.0:0.97 measured by inductive coupled plasma–optical emission spectrometry (ICP-OES, Perkin Elmer Optima 3300XL).

$LiMnPO_4$ thin films were grown on $Pt/Cr/SiO_2$ substrates (Sendai Sekiei Glass) by PLD. The fourth harmonic of a Nd:YAG laser (Spectra-Physics, LAB-150) was used with laser energy of 1.58 J cm^{-2}. The working pressure of Ar gas was fixed between 2 and 100 Pa after evacuating the chamber to 2×10^{-4} Pa, and the substrate temperature was set to 400, 500, 600, and 700 °C. The crystal structure of the $LiMnPO_4$ thin films was characterized by X-ray diffraction (XRD, Rigaku, SmartLab 90TF) using Cu K_α radiation, and in-plane measurements with $2\theta\chi/\phi$ geometry were used. The lattice vibration of the film was analyzed by Fourier transform infrared (FTIR) spectroscopy (Perkin-Elmer, Spectrum GX). The FTIR spectra were measured by an attenuated total reflectance method. The surface morphology of the thin-films was observed by a field emission scanning electron microscope (FE-SEM, Hitachi S-4800). The operating voltage of the FE-SEM was 2.0 kV. The composition ratio of the $LiMnPO_4$ thin film was measured by ICP-OES analysis. The $LiMnPO_4$ film was dissolved with aqua regia. Reference solutions were made by diluting the Li, Mn and P standard solutions (Wako Pure Chemical).

The electrochemical properties of the $LiMnPO_4$ thin films were evaluated by cyclic voltammetry (CV) using a potentiostat (Bio-Logic, SP-150). A three-electrode cell was assembled in an Ar filled grove box using $LiMnPO_4$ thin films as the positive electrode. Lithium metal was used for the counter and reference electrodes, and 1 mol L^{-1} of $LiPF_6$ was dissolved in ethylene carbonate–dimethyl carbonate (1:1 vol, Kishida Chemical) as the liquid electrolyte. The area of the $LiMnPO_4$ film was 0.56 cm^2, and the average thickness of the film was ca. 50 nm. The cell was tested by CV measurement in the range of 3.5–4.4 V vs. Li/Li^+ with a scan rate of 20 mV min^{-1}.

All solid-state TFBs, which consisted of $Li/Li_3PO_4/LiMnPO_4$, were deposited on a $Pt/Cr/SiO_2$ substrate. The conditions under which the $LiMnPO_4$ layer was deposited onto the $Pt/Cr/SiO_2$ substrate were 600 °C substrate temperature in Ar atmosphere of 100 Pa for 1 h using Nd:YAG laser. The amorphous Li_3PO_4 solid electrolyte was deposited at room temperature in O_2 atmosphere at 0.2 Pa for 3 h using an ArF excimer laser, and the Li film was deposited by thermal evaporation. Details of the Li_3PO_4 and Li depositions have been reported in a previous

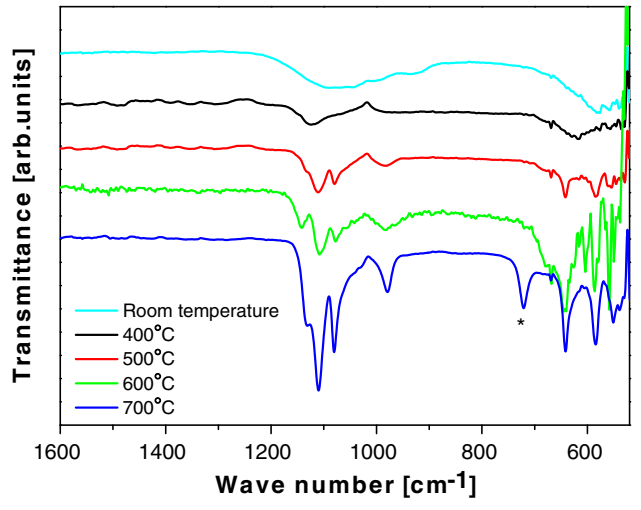

Fig. 2. FTIR spectra for $LiMnPO_4$ thin films at different substrate temperatures at 100 Pa Ar pressure. Asterisk (*) shows a peak from manganese oxide.

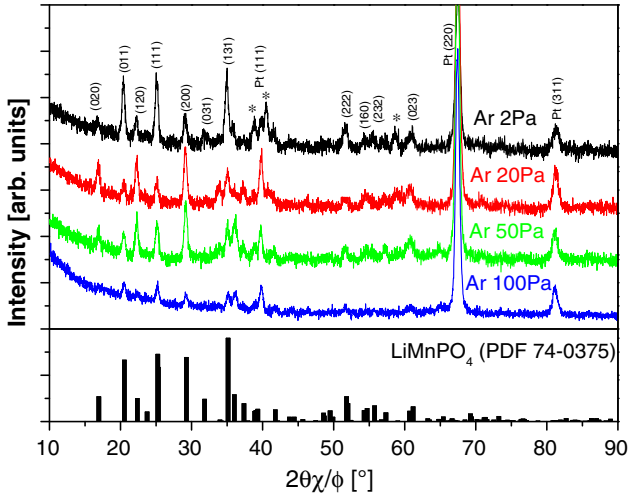

Fig. 3. In-plane X-ray diffraction patterns for $LiMnPO_4$ thin films under different atmospheric pressures at a substrate temperature of 600 °C. Asterisk (*) shows peaks probably due to manganese oxide.

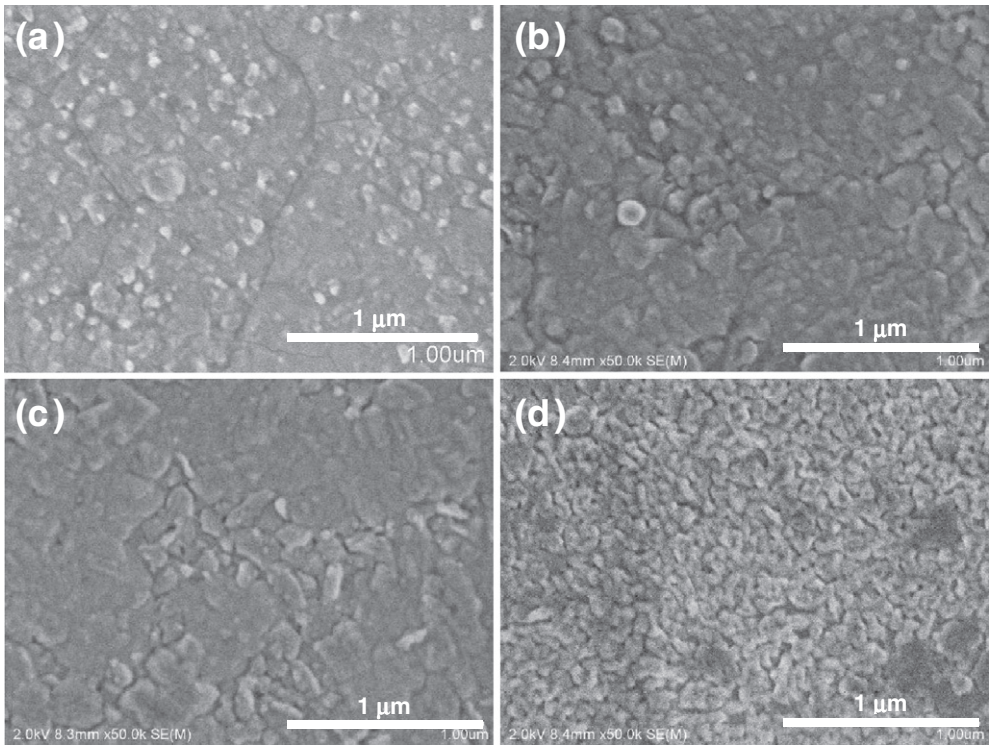

Fig. 4. FE-SEM images of $LiMnPO_4$ thin films at different atmospheric pressures at a substrate temperature of 600 °C. (a) 2 Pa, (b) 20 Pa, (c) 50 Pa, and (d) 100 Pa.

paper [15]. The area and the thickness of $LiMnPO_4$ film were 0.09 cm^2 and 50 nm, respectively. The TFBs were placed in a vacuum-tight stainless steel cell. Gold wire and silver paste were used to connect the cell and batteries electrically. CV measurement was performed at 25 °C under vacuum in the range of 3.5–4.5 V vs. Li/Li^+ with a scan rate of 20 mV min^{-1}, 50 mV min^{-1}, 1 mV s^{-1}, 2 mV s^{-1}, and

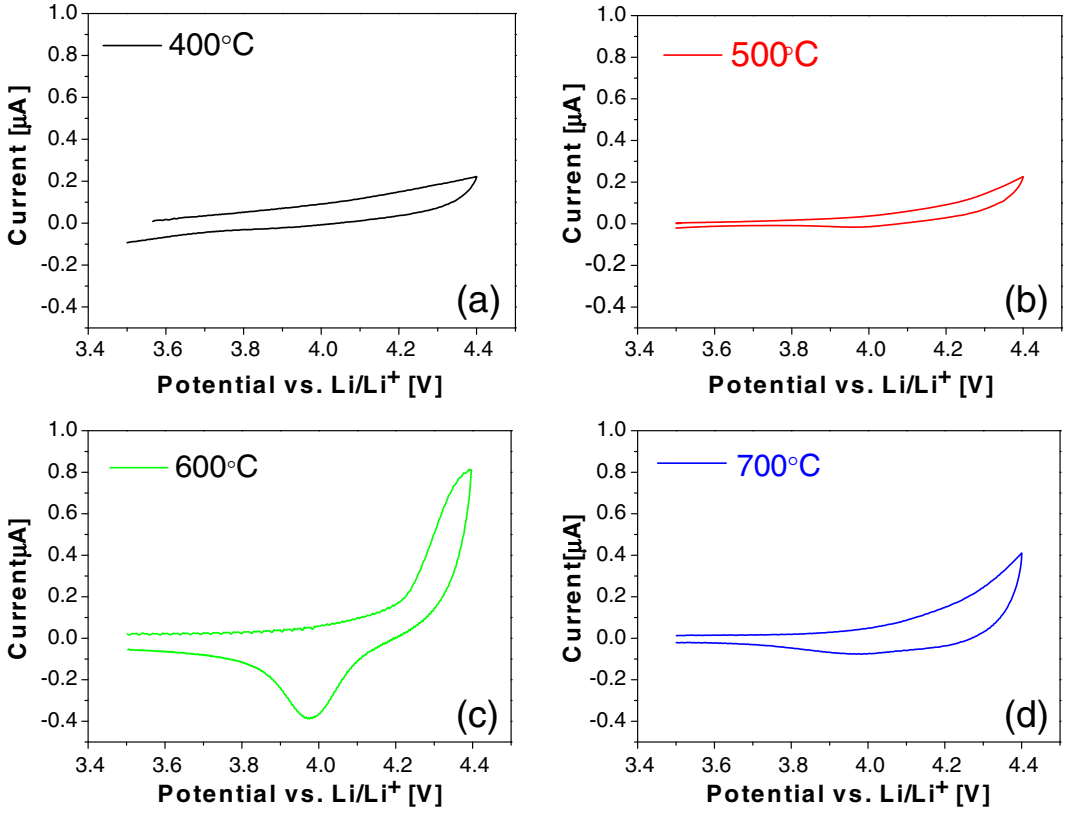

Fig. 5. Cyclic voltammograms of the films deposited at (a) 400 °C, (b) 500 °C, (c) 600 °C, and (d) 700 °C at 100 Pa Ar pressure. The CV scan rate was 20 mV min^{-1}. The films were deposited on Pt coated SiO_2 glass substrates.

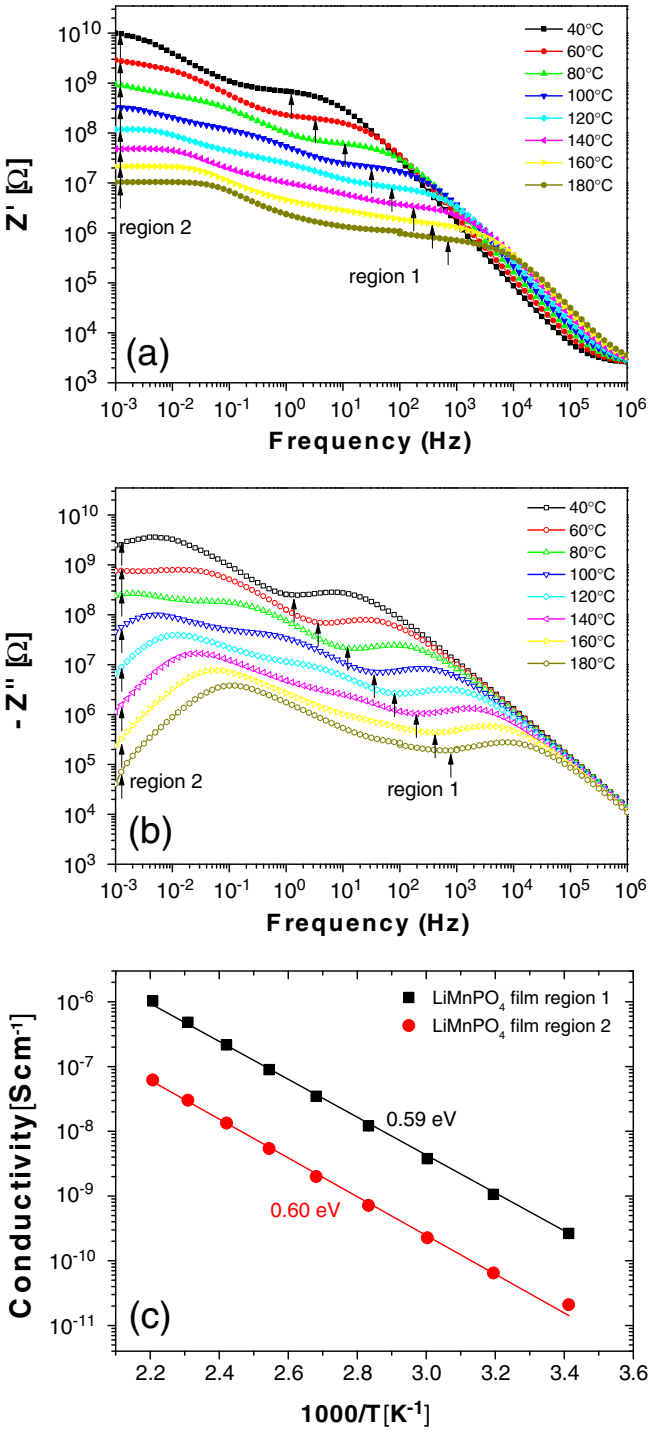

Fig. 6. The conductivity of the $LiMnPO_4$ thin film prepared at 600 °C at 100 Pa Ar pressure. The temperature dependence of (a) real and (b) imaginary part of the impedance spectra is shown. The Arrhenius plot of the conductivity is shown in (c). The two conductivities are determined from regions 1 and 2 of the impedance spectra.

5 mV s^{-1} for 50 cycles. The cycle performance of the TFB was investigated for 500 cycles with a scan rate of 20 mV min^{-1}.

3. Results and discussion

Fig. 1 shows the in-plane XRD patterns of the $LiMnPO_4$ thin films deposited at various substrate temperatures. The Ar pressure was maintained at 100 Pa, and the film deposited at 400 °C showed three peaks due to Pt reflections from the $Pt/Cr/SiO_2$ substrate. There is no Bragg reflection of $LiMnPO_4$, i.e., the $LiMnPO_4$ deposited at 400 °C was in the amorphous state. The $LiMnPO_4$ thin films deposited at 500 and 600 °C showed that several peaks that can be attributed to the Bragg reflections of crystalline $LiMnPO_4$. However, the film deposited at 700 °C indicated the decomposed phase which was possibly attributed to the manganese oxide compounds such as MnO_2 or Mn_2O_3. Thus, the crystalline, single phase $LiMnPO_4$ thin films are grown at substrate temperatures between 500 and 600 °C. The composition ratio of the $LiMnPO_4$ thin film prepared at 600 °C and 100 Pa of Ar was Li: Mn: P = 1.0 ± 0.2: 1.0: 0.88 ± 0.08 measured by ICP-OES analysis. The composition of thin film was close to the stoichiometry. The manganese was slightly higher than the phosphorous in the thin film. This result suggests the existence of manganese oxide in the thin film.

Fig. 2 shows the FTIR spectra of the $LiMnPO_4$ thin films deposited at various substrate temperatures. The films deposited at room temperature and 400 °C show broad peaks in the frequency region of 1000–1200 cm^{-1}. These peaks are attributed to the asymmetric stretching vibration (ν_3) mode of the PO_4 group [38]. The broadening of the peaks indicates that the films were amorphous. The films deposited at 500 and 600 °C show sharp bands in the frequency of 1000–1200 cm^{-1}, which corresponds to the ν_3 mode of the PO_4 group in the $LiMnPO_4$ crystal [38]. The thin film deposited at 700 °C showed the additional phase at 720 cm^{-1} that may be attributed to the stretching vibration of the MnO_6 octahedral in MnO_2 [39].

Fig. 3 shows the in-plane XRD pattern of the $LiMnPO_4$ thin films deposited at various Ar pressures at 600 °C. All the films show Bragg peaks corresponding to the reflections of the $LiMnPO_4$. Small manganese oxide peaks were found in the films grown at lower Ar pressure. In addition, the intensity of the (020) peak located at 16.9° was different for the film deposited in 100 Pa, while the films deposited under the pressure of 2–50 Pa show the (020) diffraction peak. The low intensity of the (020) peak suggests that the film grown at 100 Pa may be textured. The small intensity of the (020) plane reflection along the in-plane suggests that the (020) plane can be parallel to the substrate. Because the Li ions in $LiMnPO_4$ are aligned along the *b*-axis, the orientation with the (020) plane parallel to the substrate can provide easier lithium diffusion along the *b*-axis.

The surface morphology of the $LiMnPO_4$ films deposited in various Ar gas pressures is shown in Fig. 4. The film shows a smooth surface with small crystalline grains, and the size of crystalline grains was less than 100 nm. The grain size of the film deposited at 2 Pa Ar was small. It was less than 50 nm. The surface of the film deposited at 100 Pa Ar shows uniform grains with the grain size around 100 nm.

Electrochemical properties of the $LiMnPO_4$ thin films fabricated under various conditions were evaluated by CV using a liquid electrolyte in the three-electrode cell. Fig. 5 shows the CV curves of the films grown at different substrate temperatures in 100 Pa Ar pressure. No intercalation (discharge) peak was observed in the film deposited at 400 °C due to the amorphous nature of the film. The film deposited at 500 °C showed a broad intercalation peak at ca. 4.0 V. The maximum intercalation peak at 4.0 V due to Mn^{2+}/Mn^{3+} redox was observed in the film deposited at 600 °C. The film deposited at 700 °C shows a small discharge peak probably due to the decomposition of $LiMnPO_4$ as observed in the XRD. The electrochemical properties of $LiMnPO_4$ films were found to be strongly dependent on the substrate temperature. At low temperature crystallization is not sufficient, and at high temperature manganese oxides are formed by decomposition. Such behavior has also been observed in $LiFePO_4$ films that show optimum capacity between 500 and 600 °C [22,23].

To calculate the intercalation capacity (negative current) and deintercalation capacity (positive current) of the films, the CV curve is integrated and divided by the scan rate ν (Vs^{-1}) as follows:

$$Q = \frac{1}{\nu}\int_{V_1}^{V_2} i\, dV, \tag{1}$$

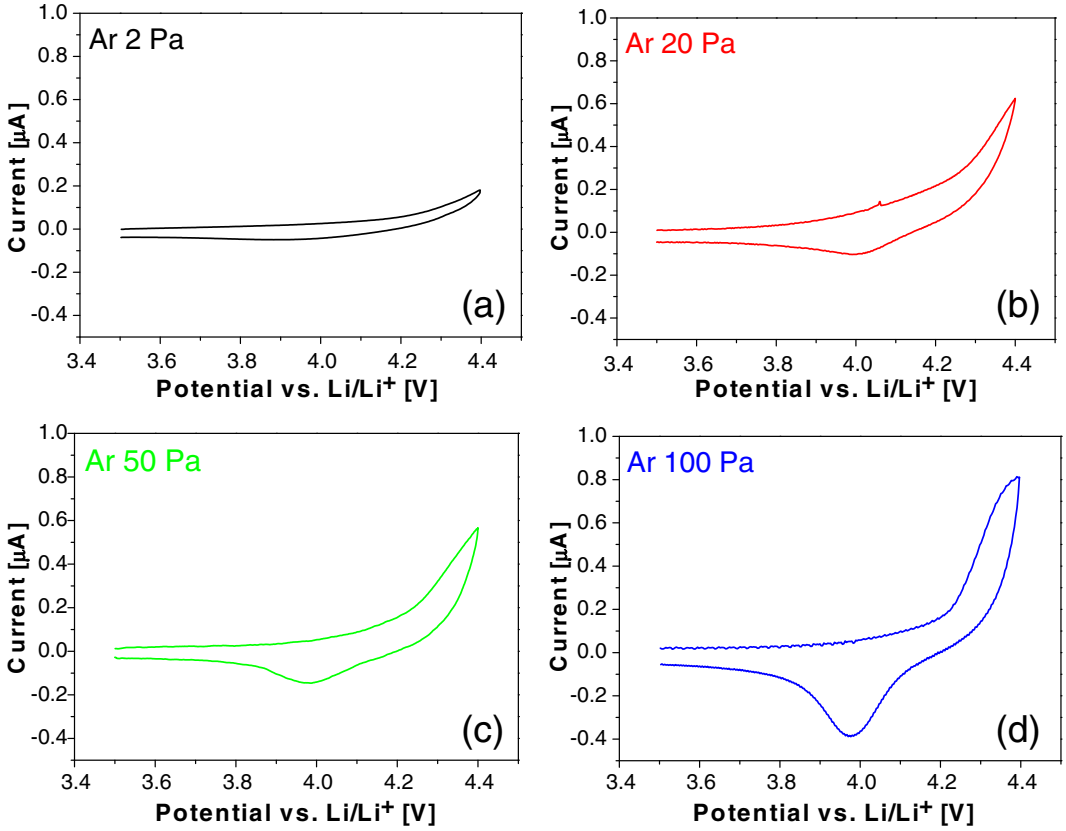

Fig. 7. Cyclic voltammograms of the films deposited in Ar at (a) 2 Pa, (b) 20 Pa, (c) 50 Pa, and (d) 100 Pa. The CV scan rate was 20 mV min^{-1}. The films were deposited on Pt coated SiO_2 glass substrates.

where Q is the charge (C), i is the current (A), and V is the potential (V). The capacity (Ah) was calculated from the charge Q using a relationship 1 Ah = 3600 C. In the case of thin-film electrodes, the capacities obtained from CV measurements agree well to the capacities obtained from constant current measurements. The weight of the thin film was measured by an ultra-microbalance (XP2U, Mettler Toledo) to calculate the specific capacity (mAh g^{-1}). The typical weight of LMP thin film was about 10 μg when the film has the thickness of about 50 nm with the area of 0.56 cm^2. The experimental errors for the weight measurements were about ±1 μg. Thus the errors for the calculated specific capacity were about ±10%.

The charge and discharge capacities of the $LiMnPO_4$ film deposited at 600 °C were 34 ± 4 and 22 ± 2 mAh g^{-1}, respectively. The reversible capacity 22 ± 2 mAh g^{-1} is 13 ± 2% of the theoretical capacity (170 mAh g^{-1}) of $LiMnPO_4$. Although the reversible capacity was smaller than the capacity of the carbon-coated $LiMnPO_4$ powder sample (150 mAh g^{-1}) [3], it was comparable or slightly higher than that of previously reported $LiMnPO_4$ films deposited by ESD [31]. Generally, the electrochemical performance of pure $LiMnPO_4$ is explained by the intrinsically poor electronic and ionic conductivities of $LiMnPO_4$ [4,5].

The electronic conductivity of the $LiMnPO_4$ thin film was measured by impedance spectroscopy using comb-type Pt electrodes. The real and imaginary parts of the impedance spectra were shown in Fig. 6(a) and (b). The film resistance can be obtained by selecting the value of the real part (Z′) at the frequency where the imaginary part (−Z″) goes through a local minimum and the real part (Z′) shows a plateau region, which is indicated by black arrows in Fig. 6(a) and (b). Two plateaus were observed at high frequency (region 1) and the low frequency (region 2). The plateau at region 2 was attributed to the electronic conductivity, because the Pt electrodes act as the ion-blocking and electron-reversible electrodes at low frequency. The plateau at high frequency region 1 may be explained as the electronic conductivity in the grain or the ionic conductivity. The blocking behavior can be explained by the grain boundary or the lithium ion-blocking Pt electrodes. The activation energy of conductivity was estimated from Arrhenius plot of conductivity as shown in Fig. 6(c). The activation energy of the conductivity region 1 (0.59 eV) agrees well with that of the region 2 (0.60 eV). The similar activation energy suggests that both conductivities come from the electronic conductivity. Another possibility is the cooperative motion of electrons and lithium ions. The electronic conductivity estimated from the region 2 was 2×10^{-11} S cm^{-1} at room temperature. Assuming that the thickness of thin film is 100 nm, the resistance of the film for 1 cm^2 area becomes 5×10^5 Ω. If the current density is 10^{-6} A, the IR drop is estimated to be 0.5 V. Therefore, the electronic resistance does not limit the electrochemical reactions.

The electronic conductivity of the bulk $LiMnPO_4$ showed different values in the literature. Wang et al. reported the electronic conductivity of 1×10^{-9} Scm^{-1} at 298 K [40]; Delacourt et al. reported much lower value which was 3×10^{-9} Scm^{-1} at 573 K [4]. The electronic conductivity of the $LiMnPO_4$ thin film was 2×10^{-11} Scm^{-1} at 298 K measured in this study. Probably, the electronic conductivity is affected by the different preparation procedure. The electronic conductivity of the $LiMnPO_4$ depends on the electronic species (holes in Mn^{3+} or electrons in Mn^{+}) accompanied with lithium or oxygen vacancies [41]. Thus, the slight deviation from the stoichiometry may cause the large difference in the electronic conductivity.

Fig. 7 shows the CV curves of the film grown at 600 °C with different Ar pressures. The discharge peak due to Mn^{2+}/Mn^{3+} redox in $LiMnPO_4$ was observed in all films. The discharge peaks gradually increased with increasing Ar pressure and attained a maximum at 100 Pa. The high capacity of the film grown at 100 Pa may be explained by different crystallographic properties. The in-plane XRD measurements reveal that the film prepared at 100 Pa showed a preferred texture, as illustrated in Fig. 3, where the (020) plane can be directed to the out-of-plane

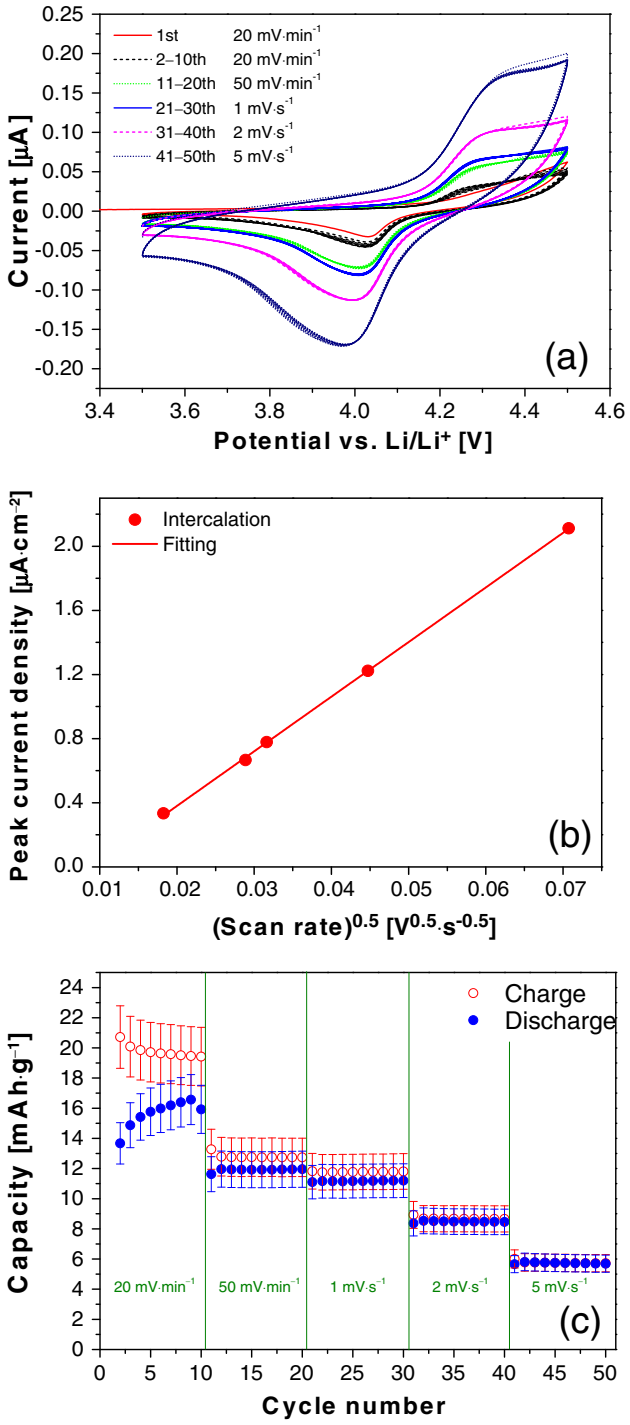

Fig. 8. CV of all solid-state thin-film batteries Li/Li_3PO_4/$LiMnPO_4$; (a) CV curves at various scan rates and (b) Randles–Sevcik plot obtained from intercalation peak of the $LiMnPO_4$ film.

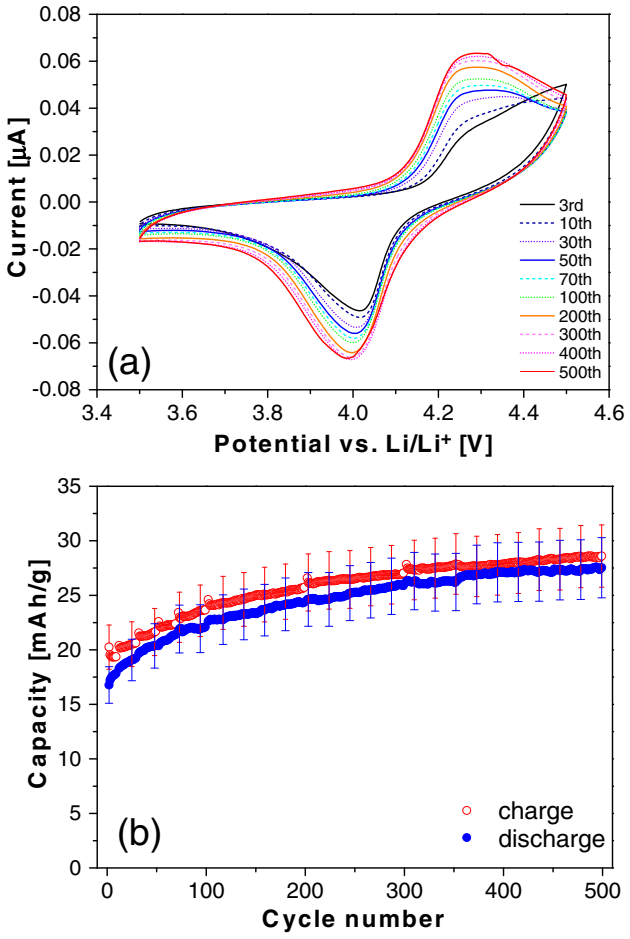

Fig. 9. CV of thin-film battery Li/Li_3PO_4/$LiMnPO_4$ for 500 cycles at 20 mV min^{-1}; (a) CV curves and (b) specific capacities of the $LiMnPO_4$ film.

to the substrate. Because the ionic motion in $LiMnPO_4$ is strongly anisotropic, this pronounced texture may increase lithium diffusion along the *b*-axis in the films grown in 100 Pa.

All solid-state TFBs were fabricated by depositing $LiMnPO_4$ as the positive electrode, amorphous Li_3PO_4 as the solid electrolyte, and Li film as the negative electrode on a Pt/Cr/SiO_2 substrate. The $LiMnPO_4$ film was deposited under optimized conditions: 600 °C substrate temperature and 100 Pa Ar pressure. The thickness of the $LiMnPO_4$ film was ca. 50 nm, and the active area was 0.09 cm^2. The weight of the active material was expected to be 1.6 μg. Fig. 8(a) shows the CV curves of the TFB, and the extraction/insertion peaks due to the Mn^{2+}/Mn^{3+} redox of $LiMnPO_4$ was observed at ca. 4.3 V and 4.0 V, respectively. Excellent reversibility was achieved by good contact between $LiMnPO_4$ and the amorphous Li_3PO_4 electrolyte as well as the $LiCoO_2$ and $LiCoMnO_4$ films [15,42]. In addition, no decomposition of the electrolyte was observed from 3.5 to 4.5 V due to the large electrochemical window of the solid electrolyte. The stable electrochemical performance is suitable for the fundamental study of the model system of $LiMnPO_4$.

Usually, the LiPON electrolyte is known as a solid electrolyte with better stability than Li_3PO_4. However, the Li_3PO_4 thin film prepared by PLD using ArF excimer laser showed good stability and ionic conductivity [15]. The electrochemical stability of Li_3PO_4 film prepared by PLD is greater than 4.7 V, while the Li_3PO_4 film prepared by RF sputtering is decomposed at 3.6 V [43]. Pyrophosphate groups with P–O–P bonds included in the Li_3PO_4 film prepared by PLD may improve the electrochemical stability.

The chemical diffusion of the $LiMnPO_4$ film was studied by CV measurements. The CV curves were obtained at different scan rates, as shown in Fig. 8(a). According to the Randles–Sevcik equation, the maximum current density i_p (A cm^{-2}) of the intercalation/deintercalation peak depends on the square root of the chemical diffusion coefficient $\tilde{D}$ (cm^2 s^{-1}) [44,45]

$$i_p = 0.4463 \cdot zFC \cdot \sqrt{\frac{zF\nu\tilde{D}}{RT}}. \quad (2)$$

Here, z denotes the valence of the mobile ions, F is Faraday's constant (C mol^{-1}), C denotes the concentration of mobile ions (mol cm^{-3}), v denotes the scan rate (V s^{-1}), R denotes the gas constant (J K^{-1} mol^{-1}), and T is temperature (K). According to Eq. (2), plotting i_p as a function of $\sqrt{v}$ should result in a straight line with a slope proportional to $\sqrt{\tilde{D}}$. For the $LiMnPO_4$ film, a Randles–Sevcik plot is shown in Fig. 8(b).

As expected, i_p depends linearly on $\sqrt{v}$, indicating a diffusion controlled process. Therefore, the chemical diffusion coefficient is calculated for the intercalation process and is found to be $\tilde{D} = 3.0 \times 10^{-17}$ cm^2 s^{-1}. This chemical diffusion coefficient value of $LiMnPO_4$ shows good agreement with the value of carbon-coated $LiMnPO_4$ nanocrystals, which was between 10^{-16} and 10^{-17} obtained by electrochemical impedance spectroscopy [3]. In contrast, the $LiFePO_4$ thin film having the same olivine structure shows chemical diffusion coefficient of approximately 10^{-13} cm^2 s^{-1}; this value was obtained by CV [22]. The chemical diffusion coefficient of the $LiMnPO_4$ thin films is four orders of magnitude smaller than the value of the $LiFePO_4$ thin film. The relatively low charge and discharge current and capacity found in this study can be explained by the low chemical diffusion coefficient of the $LiMnPO_4$ thin film.

Finally, the cycle stability of the thin-film battery is shown for 500 cycles. Fig. 9(a) shows the CV curves and Fig. 9(b) shows the specific capacity for 500 cycles. The CV curves in Fig. 8(a) clearly show the excellent cycle stability of the thin-film battery using $LiMnPO_4$ film as the positive electrode. This cycle stability results from the rigid structure of olivine-type $LiMnPO_4$ with a PO_4 framework. The specific capacity after 500 cycles was 28 ± 3 mAh g^{-1} and the volumetric capacity was 10 ± 1 μAh cm^{-2} μm^{-1}, which is $16 \pm 2\%$ of the theoretical capacity. After long term cycling, the capacity increased gradually. The unusual behavior of the capacity is due to the gradual increase of the utilization of $LiMnPO_4$. One possible explanation for this behavior is the crystallization of the remaining amorphous part, which increases the utilization of the $LiMnPO_4$ film. The other explanation is the formation of Li vacancies and electronic species (Mn^{3+}), during charge–discharge cycles. The Li vacancies and electronic species enhance the electronic conductivity of the $LiMnPO_4$. Since the utilization of $LiMnPO_4$ was limited by slow chemical diffusion coefficient, the increase in the electronic conductivity improves the utilization of $LiMnPO_4$.

4. Conclusion

An olivine-type $LiMnPO_4$ thin-film cathode was fabricated by PLD using the stoichiometric $LiMnPO_4$ target. Substrate temperature and Ar gas pressure during deposition strongly affect the film structure and electrochemical properties. A weak (020) texture observed in the in-plane XRD provides a favorable orientation for lithium diffusion in the film. The $LiMnPO_4$ thin film prepared under optimized conditions shows charge and discharge peaks at ca. 4.1 V due to Mn^{2+}/Mn^{3+} redox of $LiMnPO_4$, and the reversible capacity was 22 ± 2 mAh g^{-1} using the liquid electrolyte. The electronic conductivity of the $LiMnPO_4$ film was 2×10^{-11} S cm^{-1} at room temperature. All solid-state TFBs were fabricated using $LiMnPO_4$ film and an amorphous Li_3PO_4 electrolyte. The TFBs show the redox peak at ca. 4.1 V with excellent cycle stability. CV was applied to study the chemical diffusion of the $LiMnPO_4$ thin film using the solid-state battery. The chemical diffusion coefficient of the $LiMnPO_4$ thin film is estimated to be 3.0×10^{-17} cm^2 s^{-1}, which is about four orders magnitude smaller than the $LiFePO_4$ thin films. After long term cycling, i.e., 500 cycles, the capacity gradually increased to 28 ± 3 mAh g^{-1}. This behavior suggests the gradual increase in the utilization of the $LiMnPO_4$ thin film. The work on thin-film batteries using the other olivine materials $LiMPO_4$ (M = Fe, Co, Ni) are under investigation.

Acknowledgments

This research was conducted under a Joint Education Program between Tsinghua University and Tohoku University. This work was partly supported by the Japan Science and Technology Agency, Advanced Low Carbon Technology Research and Development Program, "Next-generation Rechargeable Battery Program." The in-plane XRD measurement was supported by "Tohoku Innovative Materials Technology Initiatives for Reconstruction" funded by the Ministry of Education, Culture, Sports, Science and Technology and the Reconstruction Agency, Japan.

References

[1] A.K. Padhi, K.S. Nanjundaswamy, J.B. Goodenough, Phospho-olivines as positive-electrode materials for rechargeable lithium batteries, J. Electrochem. Soc. 144 (1997) 1188.
[2] D. Choi, D. Wang, I.-T. Bae, J. Xiao, Z. Nie, W. Wang, V.V. Viswanathan, Y. Jung Lee, J.-G. Zhang, G.L. Graff, Z. Yang, J. Liu, LiMnPO4 nanoplate grown via solid-state reaction in molten hydrocarbon for Li-ion battery cathode, Nano Lett. 10 (2010) 2799.
[3] H.-C. Dinh, S.-I. Mho, Y. Kang, I.-H. Yeo, Large discharge capacities at high current rates for carbon-coated $LiMnPO_4$ nanocrystalline cathodes, J. Power Sources 244 (2013) 189.
[4] C. Delacourt, L. Laffont, R. Bouchet, C. Wurm, J.-B. Leriche, M. Morcrette, J.-M. Tarascon, C. Masquelier, Toward understanding of electrical limitations (electronic, ionic) in LiMPO4 (M = Fe, Mn) electrode materials, J. Electrochem. Soc. 152 (2005) A913.
[5] K. Rissouli, K. Benkhouja, J.R. Ramos-Barrado, C. Julien, Electrical conductivity in lithium orthophosphates, Mater. Sci. Eng. B 98 (2003) 185.
[6] S. Moon, P. Muralidharan, D.K. Kim, Carbon coating by high-energy milling and electrochemical properties of $LiMnPO_4$ obtained in polyol process, Ceram. Int. 38 (2012) S471.
[7] S.K. Martha, B. Markovsky, J. Grinblat, Y. Gofer, O. Haik, E. Zinigrad, D. Aurbach, T. Drezen, D. Wang, G. Deghenghi, I. Exnar, $LiMnPO_4$ as an advanced cathode material for rechargeable lithium batteries, J. Electrochem. Soc. 156 (2009) A541.
[8] T.-H. Kim, H.-S. Park, M.-H. Lee, S.-Y. Lee, H.-K. Song, Restricted growth of $LiMnPO_4$ nanoparticles evolved from a precursor seed, J. Power Sources 210 (2012) 1.
[9] T. Drezen, N.-H. Kwon, P. Bowen, I. Teerlinck, M. Isono, I. Exnar, Effect of particle size on $LiMnPO_4$ cathodes, J. Power Sources 174 (2007) 949.
[10] K. Dokko, T. Hachida, M. Watanabe, $LiMnPO_4$ nanoparticles prepared through the reaction between Li_3PO_4 and molten aqua-complex of $MnSO_4$, J. Electrochem. Soc. 158 (2011) A1275.
[11] J. Wang, X. Sun, Understanding and recent development of carbon coating on $LiFePO_4$ cathode materials for lithium-ion batteries, Energy Environ. Sci. 5 (2012) 5163.
[12] K. Kanehori, K. Matsumoto, K. Miyauchi, T. Kudo, Thin film solid electrolyte and its application to secondary lithium cell, Solid State Ionics 9–l0 (1983) 1445.
[13] N. Kuwata, J. Kawamura, K. Toribami, T. Hattori, N. Sata, Thin-film lithium-ion battery with amorphous solid electrolyte fabricated by pulsed laser deposition, Electrochem. Commun. 6 (2004) 417.
[14] Y.-S. Park, S.-H. Lee, B.-I. Lee, S.-K. Joo, All-solid-state lithium thin-film rechargeable battery with lithium manganese oxide, Electrochem. Solid-State Lett. 2 (1999) 58.
[15] N. Kuwata, N. Iwagami, Y. Tanji, Y. Matsuda, J. Kawamura, Characterization of thin-film lithium batteries with stable thin-film Li_3PO_4 solid electrolytes fabricated by ArF excimer laser deposition, J. Electrochem. Soc. 157 (2010) A521.
[16] J.B. Bates, N.J. Dudney, B. Neudecker, A. Ueda, C.D. Evans, Thin-film lithium and lithium-ion batteries, Solid State Ionics 135 (2000) 33.
[17] J. Kawamura, N. Kuwata, K. Toribami, N. Sata, O. Kamishima, T. Hattori, Preparation of amorphous lithium ion conductor thin films by pulsed laser deposition, Solid State Ionics 175 (2004) 273.
[18] Y.-N. Zhou, M.-Z. Xue, Z.-W. Fu, Nanostructured thin film electrodes for lithium storage and all-solid-state thin-film lithium batteries, J. Power Sources 234 (2013) 310.
[19] J. Hong, C. Wang, N.J. Dudney, M.J. Lance, Characterization and performance of $LiFePO_4$ thin-film cathodes prepared with radio-frequency magnetron-sputter deposition, J. Electrochem. Soc. 154 (2007) A805.
[20] K.-F. Chui, Optimization of synthesis process for carbon-mixed $LiFePO_4$ composite thin-film cathodes deposited by bias sputtering, J. Electrochem. Soc. 154 (2007) A129.
[21] J. Xie, N. Imanishi, T. Zhang, A. Hirano, Y. Takeda, O. Yamamoto, Li-ion diffusion kinetics in $LiFePO_4$ thin film prepared by radio frequency magnetron sputtering, Electrochim. Acta 54 (2009) 4631.
[22] M. Köhler, F. Berkemeier, T. Gallasch, G. Schmitz, Lithium diffusion in sputter-deposited lithium iron phosphate thin-films, J. Power Sources 236 (2013) 61.
[23] C. Yada, Y. Iriyama, S.-K. Jeong, T. Abe, M. Inaba, Z. Ogumi, Electrochemical properties of $LiFePO_4$ thin films prepared by pulsed laser deposition, J. Power Sources 146 (2005) 559.
[24] F. Sauvage, E. Baudrin, L. Gengembre, J.-M. Tarascon, Effect of texture on the electrochemical properties of $LiFePO_4$ thin films, Solid State Ionics 176 (2005) 1869.
[25] J. Sun, K. Tang, X. Yu, H. Li, X. Huang, Needle-like LiFePO4 thin films prepared by an off-axis pulsed laser deposition technique, Thin Solid Films 517 (2009) 2618.

[26] S.-W. Song, R.P. Reade, R. Kostecki, K.A. Striebel, Electrochemical studies of the $LiFePO_4$ thin films prepared with pulsed laser deposition, J. Electrochem. Soc. 153 (2006) A12.
[27] T. Matsumura, N. Imanishi, A. Hirano, N. Sonoyama, Y. Takeda, Electrochemical performances for preferred oriented PLD thin-film electrodes of $LiNi_{0.8}Co_{0.2}O_2$, $LiFePO_4$ and $LiMn_2O_4$, Solid State Ionics 179 (2008) (2011–2015).
[28] Z.G. Lu, M.F. Lo, C.Y. Chung, Pulse laser deposition and electrochemical characterization of $LiFePO_4$–C composite thin films, J. Phys. Chem. C 112 (2008) 7069.
[29] K. Tang, X. Yu, J. Sun, H. Li, X. Huang, Kinetic analysis on $LiFePO_4$ thin films by CV, GITT, and EIS, Electrochim. Acta 56 (2011) 4869.
[30] Z.G. Lu, H. Cheng, M.F. Lo, C.Y. Chung, Pulsed laser deposition and electrochemical characterization of $LiFePO_4$–Ag composite thin films, Adv. Funct. Mater. 17 (2007) 3885.
[31] J. Ma, Q.-Z. Qin, Electrochemical performance of nanocrystalline $LiMPO_4$ thin-films prepared by electrostatic spray deposition, J. Power Sources 148 (2005) 66.
[32] W.C. West, J.F. Whitacre, B.V. Ratnakumar, Radio frequency magnetron-sputtered $LiCoPO_4$ cathodes for 4.8 V thin-film batteries, J. Electrochem. Soc. 150 (2003) A1660.
[33] J. Xie, N. Imanishi, T. Zhang, A. Hirano, Y. Takeda, O. Yamamoto, Li-ion diffusion kinetics in $LiCoPO_4$ thin films deposited on NASICON-type glass ceramic electrolytes by magnetron sputtering, J. Power Sources 192 (2009) 689.
[34] A. Eftekhari, Surface modification of thin-film based $LiCoPO_4$ 5 V cathode with metal oxide, J. Electrochem. Soc. 151 (2004) A1456.
[35] J.L. Shui, Y. Yu, X.F. Yang, C.H. Chen, $LiCoPO_4$-based ternary composite thin-film electrode for lithium secondary battery, Electrochem. Commun. 8 (2006) 1087.
[36] M.S. Bhuwaneswari, L. Dimesso, W. Jaegermann, Preparation of $LiCoPO_4$ powders and films via sol–gel, J. Sol-Gel. Sci. Technol. 56 (2010) 320.
[37] N. Kuwata, R. Kumar, K. Toribami, T. Suzuki, T. Hattori, J. Kawamura, Thin film lithium ion batteries prepared only by pulsed laser deposition, Solid State Ionics 177 (2006) 2827.
[38] K.P. Korona, J. Papierska, M. Kaminska, A. Witowski, M. Michalska, L. Lipinska, Raman measurements of temperature dependencies of phonons in $LiMnPO_4$, Mater. Chem. Phys. 127 (2011) 391.
[39] Z. Weixin, R. Xiangbin, Y. Zeheng, W. Hua, W. Qiang, H. Fei, Hydrothermal synthesis of crystalline α/β-MnO nanorods via γ-MnOOH nanorod precursors, Front. Chem. Eng. China 1 (2007) 365.
[40] D. Wang, C. Ouyang, T. Drézen, I. Exnar, A. Kay, N.-H. Kwon, P. Gouerec, J.H. Miners, M. Wang, M. Grätzel, Improving the electrochemical activity of $LiMnPO_4$ via Mn-site substitution, J. Electrochem. Soc. 157 (2010) A225.
[41] Craig A.J. Fisher, Veluz M. Hart Prieto, M. Saiful Islam, Lithium battery materials $LiMPO_4$ (M = Mn, Fe, Co, and Ni): insights into defect association, transport mechanisms, and doping behavior, Chem. Mater. 20 (2008) 5907.
[42] N. Kuwata, S. Kudo, Y. Matsuda, J. Kawamura, Fabrication of thin-film lithium batteries with 5-V-class $LiCoMnO_4$ cathodes, Solid State Ionics 262 (2014) 165.
[43] X. Yu, J.B. Bates, G.E. Jellison Jr., F.X. Hart, A stable thin-film lithium electrolyte: lithium phosphorus oxynitride, J. Electrochem. Soc. 144 (1997) 524.
[44] J.E.B. Randles, A cathode ray polarograph. Part II.—The current–voltage curves, Trans. Faraday Soc. 44 (1948) 327.
[45] F.G. Lether, P.R. Wenston, An algorithm for the numerical evaluation of the reversible Randles–Sevcik function, Comput. Chem. 11 (1987) 179.